Mesonic *y* scaling

R. J. Peterson,[1] J. T. Brack,[1] Y. Fujii,[2] O. Hashimoto,[2] T. Takahashi,[2] M. Itoh,[3] and H. Sakaguchi[2]
[1]*Nuclear Physics Laboratory, University of Colorado, Boulder, Colorado 80309-0446*
[2]*Department of Physics, Tohoku University, Sendai 980-8578, Japan*
[3]*Department of Physics, Kyoto University, Kyoto 606-8502, Japan*
(Received 3 October 2001; published 17 April 2002)

The concept of *y* scaling has been demonstrated in the scattering of high-energy electrons to the nuclear continuum, demonstrating the incoherent elastic scattering of the projectile from individual bound nucleons. Scattering of intermediate energy π^- and K^+ from complex nuclei also shows scaling for cases of low density or small cross sections, but not for all nuclei. These results are used to evaluate the use of such mesonic *y* scaling as a means to measure meson-nucleon elastic differential cross sections within the nuclear medium.

DOI: 10.1103/PhysRevC.65.054601 PACS number(s): 25.80.Ls

I. INTRODUCTION

Inclusive inelastic electron scattering at high beam momenta has been shown to follow a *y*-scaling response. Under assumptions of incoherent, single nucleon elastic scattering, kinematic relations have been shown to transform spectra for a range of beam momenta and scattering angles into the same *y*-scaled responses [1,2]. The transformations of doubly differential cross sections and energy loss ω (all in the laboratory frame) at each momentum transfer q are defined to be [3]

$$y = y_\infty \left[1 - \frac{y_\infty}{2(A-1)m_N} \frac{\sqrt{m_N^2 + (q_{\rm eff} + y_\infty)^2}}{y_\infty + q_{\rm eff}} \right] \tag{1}$$

with

$$F(y) = \frac{d^2\sigma/d\Omega d\omega}{d\sigma/d\Omega({\rm free})} \frac{1}{A_{\rm eff}} \frac{q_{\rm eff}}{\sqrt{m_N^2 + (q_{\rm eff} + y)^2}}, \tag{2}$$

with

$$y_\infty = \sqrt{\tilde{\omega}(\tilde{\omega} + 2m_N)} - q_{\rm eff}, \tag{3}$$

$$\tilde{\omega} = \omega - {\rm SE},$$

$$q_{\rm eff} = q \left[1 \pm \frac{4Z\alpha\hbar c}{3Er_0A^{1/3}} \right], \quad r_0 = 1.12 \ \ {\rm fm}. \tag{4}$$

Separation energies (SE) are listed in Table I, as used in Ref. [3] or interpolated from values reported there. Free nucleon masses m_N are used throughout. At sufficiently large q, the observable y may be thought of as the component of the nucleon's internal momentum along the direction of q at the moment it was struck.

Thus we know that the nucleus offers us this *y*-scaling response $F(y)$. We here address the question of whether this scaling can be seen in the scattering of high-energy mesons, differing from the electrons in their strong interactions with nucleons and nuclei, and whether such meson data can be used to extract $d\sigma/d\Omega$, the in-medium elastic meson-nucleon differential cross section, from continuum spectra. If so, these *y*-scaling spectra would offer a direct measure of this important ''medium effect,'' searching for differences in the interactions of mesons within complex nuclei from those measured in free space.

Moreover, electron scattering has been demonstrated to show a ''superscaling'' response, whereby the continuum spectra of all nuclei have been shown to be the same under a certain transformation [3]. If similar methods can be shown to be valid for meson scattering, we could even measure the nuclear target, or density, dependence of these medium effects.

II. METHODS

Most pion data for this analysis come from Refs. [4,5], where π^- at beam momenta from 780 to 1050 MeV/c were scattered from targets of D, ^{6}Li, C, Ca, Zr, and ^{208}Pb. Momentum transfers ranged from 350 to 650 MeV/c, binned into steps 25 MeV/c wide. Some π^+ data from Ref. [6] are also used, at a beam momentum of 624 MeV/c. K^+ continuum scattering data at 715 MeV/c from Ref. [7] are used, at the maximum momentum transfer of 480 MeV/c from that work. In each case, the absolute normalization of the cross sections was very secure, being calibrated on scattering

TABLE I. Numerical values used to evaluate the scaling transformations in the text. Separation energies (SE) are from Ref. [3], or interpolated from values there. Fermi momenta for electron scattering are from Ref. [3]; those for π^- are from Refs. [4,5], and those for K^+ from Ref. [7]. All are obtained by fits to the shape of the quasielastic peak to the form of the relativistic Fermi gas, with k_f in MeV/c. Interpolated values are in parantheses. Effective numbers of nucleons are from an eikonal calculation.

Target	SE (MeV)	$k_f(ee')$	$A_{\rm eff}(\pi^-)$	$k_f(\pi^-)$	$A_{\rm eff}(K^+)$	$k_f(K^+)$
D	2.0		1.27	53	2.0	73
^{6}Li	10.0		2.66	147		
C	15.0	220	2.66	183	6.1	190
Ca	17.0	(232)	4.95	199	14.9	220
Zr	22.0	(236)	6.68	214		
Pb	25.0	240	8.68	193	33.3	230

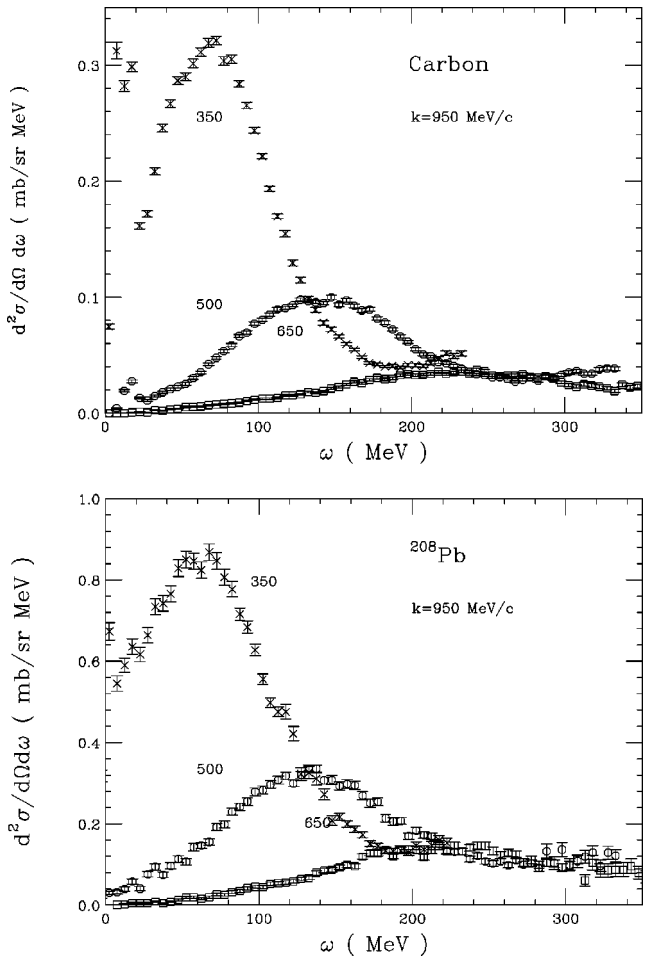

FIG. 1. Doubly differential cross sections measured for scattering of 950 MeV/c π^- from C and ^{208}Pb are shown at three values of the laboratory frame momentum transfer q [4,5]. Coherent scattering is noted at low energy losses ω, and a broad incoherent quasielastic peak dominates the continuum.

from free protons and using the known elastic cross sections [8].

Figure 1 shows representative π^- spectra for C and ^{208}Pb at three momentum transfers. The prominent quasifree peak is noted at all values of q. At 350 MeV/c we still see traces of coherent elastic and inelastic scattering at low energy losses. The energy resolution of these spectra was 2.5 MeV [full width at half maximum (FWHM)].

Since we desire to use the incoherent scattering from individual nucleons for this study, we need care with the kinematic conditions. These are spelled out in Chap. 11 of Ref. [9]. The momentum transfer q must satisfy both

$$q \gg \sqrt{8mT/3} \cong 255 \ \text{MeV}/c$$

and

$$q^2/2m \gg |U| = 40 \ \text{MeV},$$

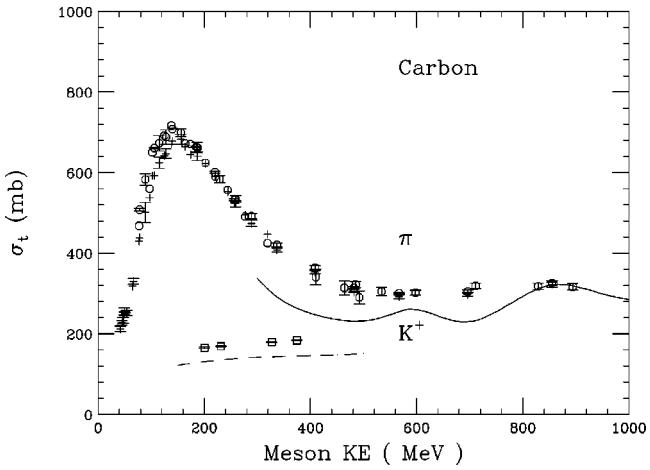

FIG. 2. The world's supply of π-carbon total cross sections is shown, with circles for π^- and crosses for π^+ [11,12]. Above the delta resonance the solid line shows results from the eikonal method used here to compute A_{eff} in Eq. (2). Squares show K^+-carbon total cross sections [15], with a corresponding eikonal theory curve.

with T the nucleon Fermi level in the nucleus and U the average nucleon-nucleus potential. At the nominal momentum transfer of $q = 500$ MeV/c, the first is probably, but not decisively, satisfied.

The beam momentum k, both incoming and outgoing, must satisfy $1/k \ll L$, the mean spacing between nucleons, with about 1.9 fm between the centers of objects each about 0.6 fm in radius. This scale requires $L = 0.7$ fm, or $k \gg 280$ MeV/c. If nucleons were larger in the nucleus than in free space, with smaller spacings between their surfaces, this standard becomes stricter. We study the low density examples of D and ^{6}Li to vary these densities or spacings.

The effective number of nucleons A_{eff} sensed by the mesonic beams is less than the total number in the nuclear targets because of absorptions and distortions. This quantity is here computed by a Glauber or eikonal method [10], compared to the present pion data in Ref. [4] and to K^+ data in Ref. [7]. A different set of geometrical parameters for the target nuclei is used here, compared to Ref. [4], so values for A_{eff} differ slightly. Meson-nucleon total cross sections used for these calculations are from Ref. [8], evaluated for each nucleus including the nuclear Coulomb effect on the beam energy and averaged over neutrons and protons. Values of A_{eff} are listed in Table I.

Resonances in the fundamental π-nucleon cross sections are a prominent feature in the beam energy range we cover. Within a complex nucleus, however, these resonances other than the delta are not visible in measurements of total cross sections [14], compared to an eikonal calculation. Figure 2 shows the world data set for carbon [11,12] compared to a curve computed for energies above 300 MeV by the eikonal method. Bumps expected from free space interactions are not found for the carbon target, but the overall agreement with the magnitude of the data confirms the reliability of the eikonal method we use at our beam energies near 800 MeV. A similar conclusion was reached in an isobar model of pion-nucleus total cross sections between 400 and 1000 MeV [13],

with theoretical cross sections somewhat lower than those shown here. Also shown in Fig. 2 are K^+-nucleus total cross sections [14], and the eikonal calculation.

Meson-nucleon differential cross sections appearing in Eq. (2) were computed from a standard phase shift analysis, kept up-to-date with the latest data [8]. Coulomb effects from the nuclear targets were included to select the beam energies for these evaluations. Except at $y=0$, the meson is colliding with a moving nucleon, and the scattering is off the mass shell. The method of evaluating such off-shell cross sections in the optimum frame [15] minimizes the difference between on and off-shell scattering. For the extreme cases in the data of Fig. 1, we find differential cross sections for the $q=650$ MeV/c case to vary by no more than 4% across the full range of the spectrum for the range of beam energies appropriate to the optimum reference frame for each energy loss ω. For $q=500$ MeV/c differential cross sections are 12% higher at the low energy loss side for $\omega=30$ MeV, and larger by 29% for the large energy loss limit of $\omega=260$ MeV. Since the resonances that provide these variations are damped within the nuclear targets, and since the effects are not large, we use only free space differential elastic π-nucleon cross sections in Eq. (2), averaged over neutrons and protons in the complex nucleus.

Electron scattering y-scaling responses can sense either the proton charges incoherently or the (largely) isovector magnetic moments. Our meson scattering is sensitive primarily to an isoscalar, nonspin, coupling to the nucleons in the nuclear medium, with about 60% of the cross section at $q=500$ MeV/c [8]. The smaller pieces do not include any term from pion exchange; the mesons scatter from nucleons only with a short range interaction. If a single meson were responsible for the largest part of the π-N interaction, it would be the putative sigma.

III. RESULTS

The transformations of Eqs. (1)–(4) have been applied to π^- spectra such as shown in Fig. 1 to form the y-scaling plots of Figs. 3 and 4. Only spectra at selected values of q have been used here. The incoherent quasifree peak is found, centered very near $y=0$. In contrast to some electron scattering spectra, these pion data also decrease and scale at positive y. This is because the small scattering angle has precluded spin transfers, and thus quenched pion production which destroys the y scaling for transverse electron scattering for $y>0$.

The very light nuclei D and ^{6}Li show very good scaling responses. The sharp peaks near $y=-130$, -180, and -210 MeV/c in the D spectra are from elastic deuteron scattering. The ^{6}Li sample shows good scaling down to $y=-200$ MeV/c.

For the carbon sample, however, scaling is not observed for q less than about 500 MeV/c. The heavier targets show decreasing agreement with the scaling hypothesis, even at large q.

Another way to sense y scaling is by plotting spectra at fixed q, but varying beam energy and scattering angle. Figure 5 shows π^- data from the same experiment as Refs. [4,5], as well as π^+ data from Ref. [6]. Scaling is only approached for the higher beam momenta, as we might expect from the kinematic conditions. Note that the free π-nucleon cross sections are changing strongly in this resonance range of beam momenta. Although optimum frame considerations [15] will

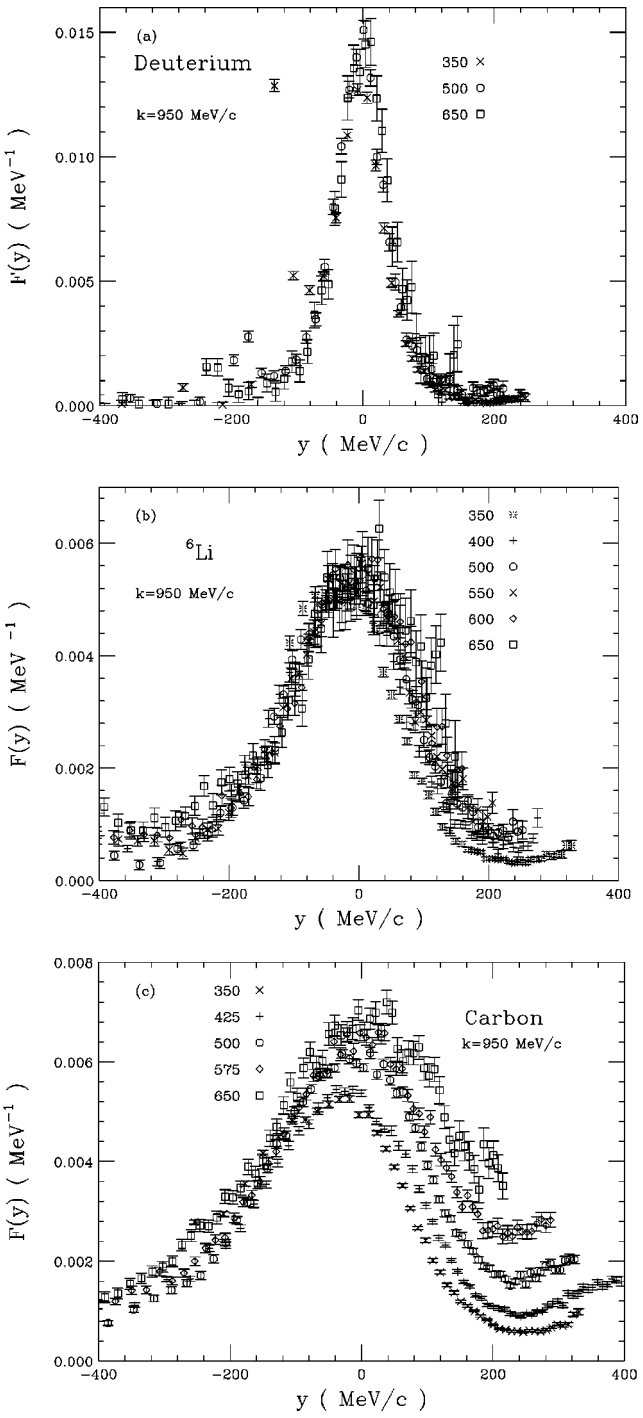

FIG. 3. Scaling functions for 950 MeV/c π^- scattered from light nuclei are shown at selected values of the momentum transfer q. The sharp peaks near $y=-130$, -180, and -210 MeV/c in the deuteron spectra are from elastic deuterium scattering. The D and ^{6}Li spectra show good y-scaling responses, but the carbon case scales only for larger values of q. Data are from Ref. [4].

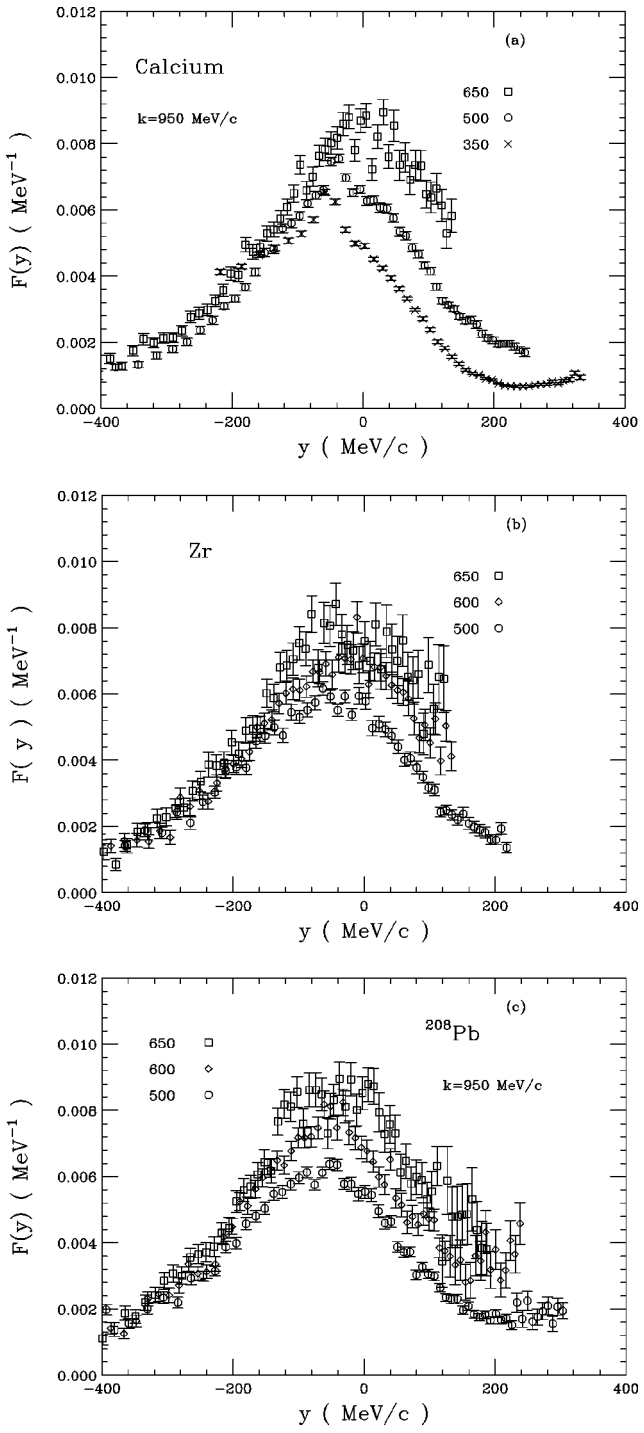

FIG. 4. Scaling functions for the heavier nuclei of our study are shown. The spike atop the Ca spectrum at $q=350$ MeV/c is the result of some hydrogen contamination in the sample. These cases do not show y scaling except near the largest values of q obtained in our measurements. Data are from Ref. [4].

be more important at the lower beam energies, they have no effect at $y=0$.

Scaling responses should be approached from below as the momentum transfers increase [1]. Figure 6 shows these approaches for the light targets at $y=0$ and at $y=-100$ MeV/c. In a similar plot of electron scattering y-scaling responses, the charge response is found to be near $F(y=0)=0.0027$ MeV^{-1} for carbon [1].

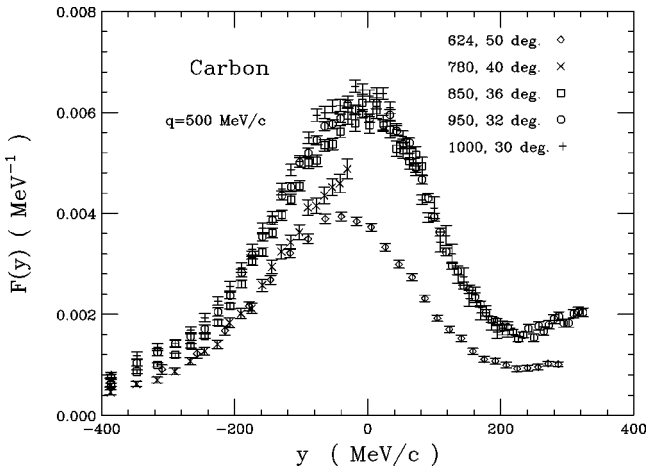

FIG. 5. Scaling spectra are shown for $q=500$ MeV/c at five combinations of beam momentum and scattering angle. The four highest π^- curves are from Refs. [4,5], while the 624 MeV/c case is for π^+ [6]. Scaling is only apparent for the higher beam momenta.

Longitudinal electron scattering responses for carbon were treated with the same scaling transformations used here for pions. Specifics used here are described in the Appendix. Data from Ref. [16] at $q=400$ and 550 MeV/c result in the scaling responses shown in Fig. 7, with magnitudes much as shown in other analyses of these data with not exactly the scaling transformation used here [17,18]. The π^- scaling responses for carbon scale much as these electron data, but with a magnitude larger by a factor of 3.5. This will be

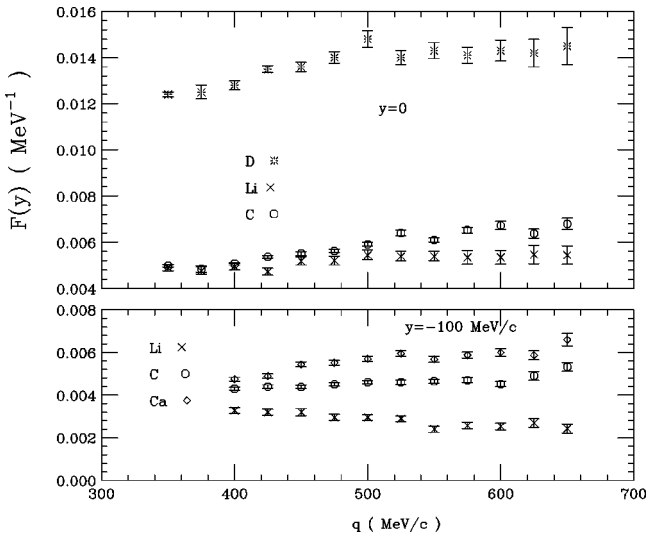

FIG. 6. Values of the scaling data at $y=0$ and $y=-100$ MeV/c are shown for the light nuclei for each of the bins of momentum transfer measured in our experiment [4]. Results for D and ^{6}Li approach an equilibrium value, while $y=0$ values continue to increase with q for C. No Ca data are shown for $y=0$ because of some hydrogen contamination in the target.

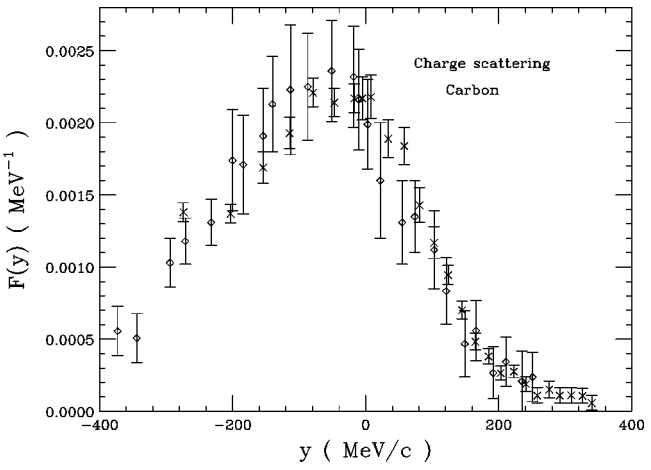

FIG. 7. Separated longitudinal electron scattering response data for carbon are transformed by the methods of this work to the y-scaling format. Crosses are for 400 MeV/c and diamonds for 550 MeV/c from Ref. [16].

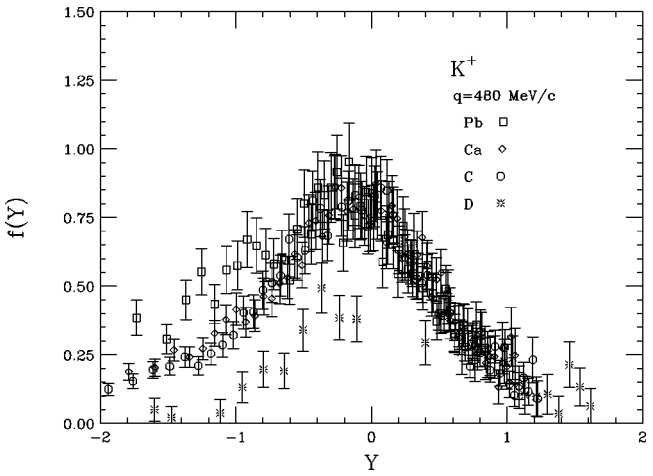

FIG. 8. Continuum K^+ spectra at $q=480$ MeV/c are shown transformed as in the text to the superscaling format. Although statistical uncertainties are large, these data do superscale. Data are from Ref. [7].

discussed in Sec. V. A difference in the location of the scaling maximum is also noted in comparing Figs. 7 and 3(c).

IV. SUPERSCALING

A means to compare a larger body of meson and electron scattering results is by way of the concept of ''superscaling'' [3]. The y-scaling resonses are further transformed by

$$Y=y/k_f, \tag{5}$$

$$f(Y)=k_f F(y). \tag{6}$$

In Ref. [3] the required Fermi momenta k_f were obtained from fits of the shape for a relativistic Fermi gas to the widths of the electron scattering quasielastic peaks; values are listed in Table I. The π^- data were also so fitted [4], as were the K^+ data [7]. This form was also used for D, although the Fermi gas model is not appropriate. Results are compared in Table I. The π^- interact at larger radii and lower density and lower Fermi momenta than the K^+ and the electrons.

Figure 8 shows the K^+ superscaling responses at $q=480$ MeV/c, the largest momentum transfer reached in that experiment [7]. Although statistical error bars are large, these data scale well near $y=0$, for $y>0$, and (except for Pb), for $y<0$. Although several data points for D seem to lie below the trend for the other targets, these are fluctuations because of poor statistical accuracy. Many of the D points are in the same band as the many other points, and hard to distinguish. In the simplest nonrelativistic Fermi gas model, with all scaling conditions met, the universal superscaling response would be a parabola reaching between $Y=-1$ and $+1$, with a magnitude of 0.75.

In Fig. 9 we show π^- superscaling responses at $q=500$, 600, and 650 MeV/c. These data seem to approach a uniform response for heavier targets. Uncertainties in the Fermi momenta used for this analysis will not change the magnitude of these plots by more than 10%. Cross sections for D and ^{6}Li track remarkably closely.

In Fig. 10 the values of $f(Y)$ are plotted for each target mass for K^+ and π^- at $Y=0$ and for π^- at $Y=-0.5$. Longitudinal electron scattering responses for C [16], Ca [19], and Fe [17] were transformed by the present usages to the superscaling responses shown in Fig. 11. Pion, K^+, and longitudinal electron superscaling responses are very similar, but the pion data are larger by a factor of 3 than the electron data, and the K^+ data are larger by a factor of 1.8.

For both y-scaling and superscaling responses, we find the meson responses to exceed those measured with electrons. Might this be evidence for a ''medium dependence''?

V. DISCUSSION

It was observed in the electron scaling and superscaling responses that longitudinal (charge) scattering data scaled well, but transverse ($S=1$, $T\simeq 1$) data increase with q [1,3]. Pion scattering also shows a sensitivity to $S=1$ scattering, roughly proportional to $\sin^2(\theta)$ where θ is the π^--N center-of-mass scattering angle for quasifree scattering [8]. The approaches to scaling at a fixed beam momentum of 950 MeV/c shown in Fig. 6 could also be thought to indicate this, since the increase in q is provided by larger scattering angles, but the increase is far below proportionality to $\sin^2\theta$. The scaling data at fixed q with varying beam energy shown in Fig. 5, however, indicate otherwise; $F(y)$ at its maximum decreases with scattering angle for the lowest beam momentum. The present data set at lower energies is limited in its kinematic suitability to the scaling hypothesis, but we conclude that we can provide no evidence for $S=1$ enhancements with pions.

It is striking that our pion y scaling and superscaling responses lie above similar results from electron scattering, by about a factor of 3. A major difference in the analyses is our need to use both computed values of $d\sigma/d\Omega$ and $A_{\rm eff}$ in Eq. (2). If in-medium π-N total cross sections increase, $A_{\rm eff}$ de-

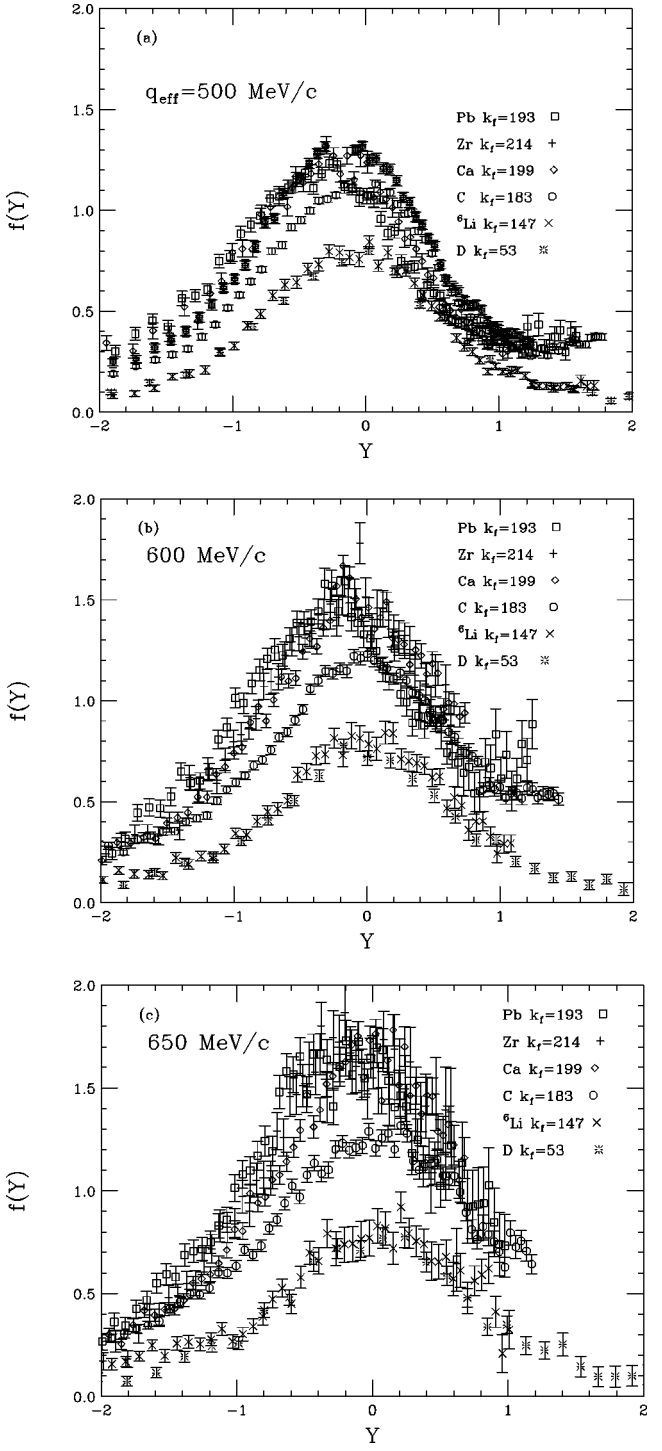

FIG. 9. Superscaling data for π^- for all of our samples are shown at three values of the effective momentum transfer. All show the same trend, shifting somewhat to lower values of Y and increasing to saturation for heavier nuclei.

crease. The eikonal model used to compute A_{eff} assumes only small angle collisions with negligible energy losses. This model is used here for angles as large as 45°, and may not be reliable for heavy nuclei. This could explain the observed failure to scale for larger momentum transfers. In particular, the outgoing pion energy for the case of 624 MeV/c is such

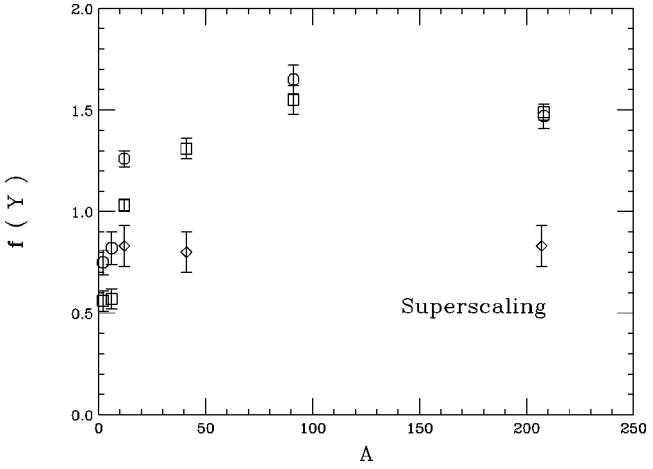

FIG. 10. At our largest effective momentum transfer $q_{\text{eff}} = 650$ MeV/c, the superscaling responses are plotted for each nuclear target for $Y=0$ for K^+ (diamonds) and π^- (circles), and for $Y=-0.5$ for π^- (squares). A rise to a saturating value is seen. Longitudinal electron scattering superscaling responses are near 0.5 at $Y=0$.

as to incur a larger probability of a second scattering than is provided by the eikonal method; this would lead to a smaller value of A_{eff} and would raise the diamond points in Fig. 5.

If differential cross sections increase in proportion to total cross sections, the product in the denominator of Eq. (2) changes little. This is demonstrated in Fig. 12, showing free $d\sigma/d\Omega$ for $q=500$ and 650 MeV/c and A_{eff} computed for π^- in the eikonal method using free-space total cross sections for a range of beam energies. Resonances are seen in both terms of the denominator of Eq. (2), but with a product that varies too slowly to be the cause of our excess in $F(y)$ and $f(Y)$ near 820 MeV. No resonances are found for the K^+-N system near our beam momentum. Both differential elastic and total K^+-nucleus cross sections are above expectations based on free K^+-N scattering, and again the mutual

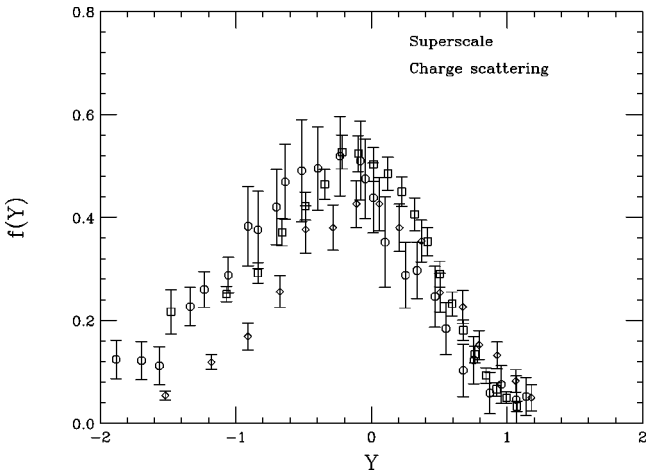

FIG. 11. Separated longitudinal electron scattering response data are superscaled by the methods of this work. Circles are for carbon at $q=550$ MeV/c [16], squares for Ca at 400 MeV/c [19], and diamonds for Fe at 570 MeV/c [17].

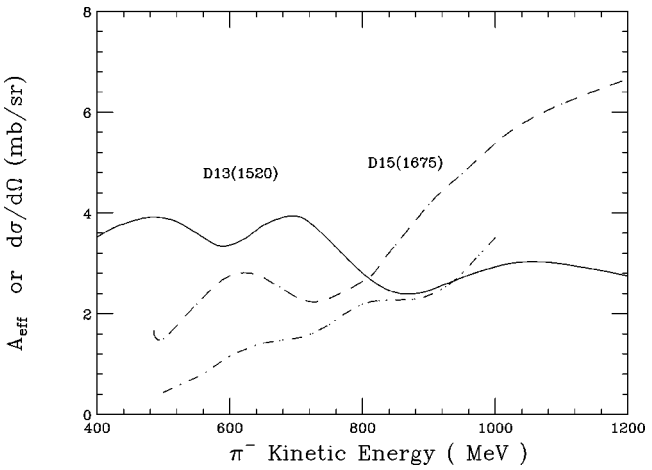

FIG. 12. The solid curve shows $A_{\rm eff}$ computed in our eikonal model, reflecting the large free π-N total cross sections near two prominent resonances. Pi-N isospin averaged differential cross sections at $q=500$ MeV/c and 650 MeV/c are also shown, as dashed and dot-dashed curves, the latter multiplied by 2. Their product, as appears in the denominator of Eq. (2), changes little. If medium effects altered both π-N total and differential cross sections equally, our scaling responses would show little sensitivity to changes from free-space values.

changes will have little effect on the magnitude of the K^+ scaling.

The present analysis finds that continuum π meson scattering does exhibit y scaling for light nuclei, but fails for larger systems. K^+ data do seem to superscale. The magnitudes of $f(Y=0)$ for pions are larger than observed with electrons by a factor of 3, while for K^+ the maximum is larger than found for electrons by a factor of 1.8. The longer mean free path of K^+ within nuclei gives them a penetration intermediate between pions and electrons. Pion responses at large q do show a larger continuum for $y>0$ than do electron charge responses.

If the radial extent of nucleons in the interior were to increase, an effect hypothesized to account for a large body of K^+ data [20], but their ingredients remain the same, we might suppose that π-N total cross sections in the nuclear medium do not increase, nor do values of $A_{\rm eff}$. Diffraction of the pions around a larger radius R would concentrate the in-medium differential cross sections to smaller angles and increase their magnitude at fixed values of qR. By this means the resulting $F(y)$ and $f(Y)$ would increase in our range of energies and angles, as noted in the data.

We have definitely seen some ''medium effect'' in mesonic y scaling in differential cross sections. This result is apparently more sensitive to medium effects than shown by the 31–42 % increase in π-N interaction strength in all channels estimated from total cross sections [13]. The failure to scale for heavy nuclei may indicate an inadequacy in the methods used to generate scaling functions, but enhancements are also seen for light nuclei exhibiting good scaling. Data at higher beam energies may remove this kinematic impediment in the future and provide a surer reaction mechanism.

ACKNOWLEDGMENTS

We wish to thank all collaborators in KEK E352 for assistance in obtaining the data used here. R.J.P. thanks T. W. Donnelly and D. B. Day for useful comments. This work was supported in part by the United States Department of Energy.

APPENDIX

Separated longitudinal electron scattering responses are often shown in the literature, and several methods have demonstrated how these scale and superscale [1]. In the present work, the transformations given in the body of the paper transform cross sections. Here we specify how we scale published electron responses to generate the data shown in Figs. 7 and 11, for a clear comparison of the data using several projectiles.

Responses R_L are defined from separated electron scattering longitudinal cross sections using the Mott electron-nucleon cross section. Scaling responses use the actual electron-nucleon elastic diferential cross sections, including the proton form factor for longitudinal or charge scattering. Here we use the dipole charge form factor for the proton, with $a_p=840$ MeV/c. With $Q^2=q^2-\omega^2$ we create longitudinal scaling functions by

$$F(y)=R_L(q,\omega)\frac{K}{Z}\left(\frac{Q}{q}\right)^4\left(1+\frac{Q^2}{4m_N^2}\right)\left(1+\frac{Q^2}{a_p^2}\right)^4 \quad \text{(A1)}$$

with $R_L(q,\omega)$ from the literature, Z as the nuclear charge, and K as in Eq. (2). Superscaling functions are created in the same fashion as used for mesons, with k_f from published fits to the widths of electron scattering quasifree cross sections.

[1] D. B. Day, J. S. McCarthy, T. W. Donnelly, and I. Sick, Annu. Rev. Nucl. Part. Sci. **40**, 357 (1990).
[2] J. Arrington *et al.*, Phys. Rev. Lett. **82**, 2056 (1999).
[3] T. W. Donnelly and I. Sick, Phys. Rev. C **60**, 065502 (1999).
[4] Y. Fujii *et al.*, Phys. Rev. C **64**, 034608 (2001).
[5] Y. Fujii, Ph.D. thesis, Tohoku University, 1998.
[6] J. E. Wise *et al.*, Phys. Rev. C **48**, 1840 (1993).
[7] C. M. Kormanyos *et al.*, Phys. Rev. C **51**, 669 (1995).
[8] R. A. Arndt and L. D. Roper, program SAID (unpublished); R. A. Arndt, J. M. Ford, and L. D. Roper, Phys. Rev. D **32**, 1085 (1985).
[9] M. L. Goldberger and K. M. Watson, *Collision Theory* (Wiley, New York, 1964).
[10] J. Ouyang, S. Hoibraten, and R. J. Peterson, Phys. Rev. C **47**, 2809 (1993).
[11] R. J. Peterson, Few-Body Syst., Suppl. **9**, 17 (1995).
[12] C. J. Gelderloos *et al.*, Phys. Rev. C **62**, 024612 (2000).

[13] C. M. Chen, D. J. Ernst, M. F. Jiang, and M. B. Johnson, Phys. Rev. C **52**, 485 (1995).
[14] E. Friedman, A. Gal, and J. Mares, Nucl. Phys. **A625**, 272 (1997).
[15] S. A. Gurvitz, Phys. Rev. C **33**, 422 (1986).
[16] P. Barreau *et al.*, Nucl. Phys. **A402**, 515 (1983).
[17] J. Jourdan, Nucl. Phys. **A603**, 117 (1996).
[18] J. M. Finn, R. W. Lourie, and B. H. Cottman, Phys. Rev. C **29**, 2230 (1984).
[19] C. F. Williamson *et al.*, Phys. Rev. C **56**, 3152 (1997).
[20] R. J. Peterson, Phys. Rev. C **60**, 022201(R) (1999).